Biomaterials 33 (2012) 1489–1499

Contents lists available at SciVerse ScienceDirect

Biomaterials

journal homepage: www.elsevier.com/locate/biomaterials

Tumor accumulation and antitumor efficacy of docetaxel-loaded core-shell-corona micelles with shell-specific redox-responsive cross-links

Ahn Na Koo [a,1], Kyung Hyun Min [b,1], Hong Jae Lee [a], Sang-Uk Lee [c], Kwangmeyung Kim [d], Ick Chan Kwon [d], Sun Hang Cho [e], Seo Young Jeong [b], Sang Cheon Lee [a,*]

[a] Department of Maxillofacial Biomedical Engineering & Institute of Oral Biology, School of Dentistry, Kyung Hee University, 1 Hoegi-dong, Dongdaemun-gu, Seoul 130-701, Republic of Korea
[b] Department of Life and Nanopharmaceutical Science, Kyung Hee University, 1 Hoegi-dong, Dongdaemun-gu, Seoul 130-701, Republic of Korea
[c] Department of Basic Pharmacy, Kyung Hee University, 1 Hoegi-dong, Dongdaemun-gu, Seoul 130-701, Republic of Korea
[d] Center for Theragnosis, Biomedical Research Institute, Korea Institute of Science and Technology, 39-1 Hawolgok-dong, Seongbuk-gu, Seoul 136-791, Republic of Korea
[e] Biomaterials Research Center, Korea Research Institute of Chemical Technology, 100 Jang-dong, Yuseong-gu, Daejeon 305-600, Republic of Korea

ARTICLE INFO

Article history:
Received 22 October 2011
Accepted 10 November 2011
Available online 29 November 2011

Keywords:
Shell cross-linking
Disulfide
Redox-responsive
Polymer micelle
Docetaxel

ABSTRACT

A robust core-shell-corona micelle bearing redox-responsive shell-specific cross-links was evaluated as a carrier of docetaxel (DTX) for cancer therapy. The polymer micelles of poly(ethylene glycol)-*b*-poly(L-lysine)-*b*-poly(L-phenylalanine) (PEG-PLys-PPhe) in the aqueous phase provided the three distinct functional domains: the PEG outer corona for prolonged circulation, the PLys middle shell for disulfide cross-linking, and the PPhe inner core for DTX loading. The shell cross-linking was performed by the reaction of disulfide-containing cross-linkers with Lys moieties in the middle shells. The shell cross-linking did not change the micelle size or the spherical morphology. The shell cross-linked micelles exhibited enhanced serum stability. The DTX release from the DTX-loaded disulfide cross-linked micelles (DTX-SSCLM) was facilitated by increasing the concentration of glutathione (GSH). At an intracellular GSH level, DTX release was facilitated due to the reductive cleavage of the disulfide cross-links in the shell domains. The in vivo tissue distribution and tumor accumulation of the DTX-SSCLM that were labeled with a near-infrared fluorescence (NIRF) dye, Cy5.5, were monitored in MDA-MB231 tumor-bearing mice. Non-invasive real-time optical imaging results indicated that the DTX-SSCLM exhibited enhanced tumor specificity due to the prolonged stable circulation in blood and the enhanced permeation and retention (EPR) effect compared with the DTX-loaded non-cross-linked micelles (DTX-NCLM). The DTX-SSCLM exhibited enhanced therapeutic efficacy in tumor-bearing mice compared with free DTX and DTX-NCLM. The domain-specific shell cross-linking that is described in this work may serve as a useful guidance for enhancing the antitumor therapeutic efficacy of various polymer micelles and nano-aggregates.

© 2011 Elsevier Ltd. All rights reserved.

1. Introduction

Nanocarriers with a high therapeutic efficacy have been developed based on self-assembled nanoparticles that can efficiently deliver anti-cancer drugs, genetic drugs, and proteins to target disease tissues [1–6]. Currently, the research trends have been shifted toward the enhancement of the delivery efficiency of major nanocarriers such as polymer micelles and polymer nano-aggregates with a core-shell structure [7–9]. Polymer micelles have presented many benefits for cancer chemotherapy due to their effective resistance to rapid renal clearance and non-specific uptake by the reticuloendothelial system (RES) [10,11]. This property enables the micellar passive targeting and enhanced permeability and retention (EPR) effect for effective tumor therapy [12–14]. To satisfy the prerequisites for successful cancer therapy, the polymer micelles need to have the following properties: high stability in blood, minimized drug loss before reaching the target tissues, an enhanced accumulation in the tumors by the EPR effect, and the facilitated release of loaded drugs within the tumor cells. However, most polymer micelles suffer from low structural stability, and the drug release is initiated upon intravenous administration, which results in drug loss at unwanted sites [15,16].

To date, the shell or core cross-linking of the polymer micelles (CLM) is a research target of great significance because this

* Corresponding author.
E-mail address: schlee@khu.ac.kr (S.C. Lee).
[1] These authors contributed equally to this work.

0142-9612/$ – see front matter © 2011 Elsevier Ltd. All rights reserved.
doi:10.1016/j.biomaterials.2011.11.013

approach can enable the polymer micelles to satisfy the above-mentioned prerequisites; thus, it cannot only enhance micellar stability but also can induce specific intracellular drug release. Our recent research has focused on ketal cross-linked or mineral-reinforced polymer micelles and has demonstrated an enhanced robustness and the facilitated release of entrapped anti-cancer drugs within cytoplasm [7,17].

The intracellular concentration of glutathione (GSH) (~ 10 mM), a thiol-containing tripeptide that cleaves disulfide bonds by a redox reaction, is known to be substantially higher than the level in the extracellular environment (~ 2 μM) [18]. This dramatic difference in the GSH concentrations has been utilized as a trigger for the intracellular delivery of bioactive agents including drugs, genes, and proteins [19–22]. For example, disulfide cross-linked micelles within shell or core domains have been used to encapsulate various drugs for intracellular delivery [22,23]. For the CLM to be useful practically, the first consideration is to tailor the polymer design for the non-toxic biodegradable CLM. However, most of the CLM systems were based on non-degradable polyacrylate or polystyrene with limited biocompatibility [23–25]. Secondly, cross-linking should be rationally localized to preserve the long-circulating property of the nanocarriers or the cross-linking efficiency. Currently, micelles with a core-shell structure are used for shell or core cross-linking. It should be noted that the shell cross-linking modifies the structure of the outer shells and thus limits the fluidity or hydration of the nanocarriers, thereby reducing prolonged circulation. In addition, in the case of core cross-linking, the links were formed within the cores, which reduced the efficiency of cross-linking due to the interference by entrapped drug molecules [26].

Herein, we demonstrated the effect of shell-specific disulfide cross-links on the tumor accumulation and the antitumor efficacy of core-shell-corona micelles loaded with docetaxel (DTX), a hydrophobic anti-cancer drug. Our primary goal was to verify the assumption that the disulfide cross-links in the middle shell can enhance the tumor targeting ability and the therapeutic efficacy of non-cross-linked native micelles. In a previous report, we reported on a fundamental study of disulfide cross-linked micelles, and the research scope was limited in the feasibility of shell cross-linking and in the evaluation of in vitro cytotoxicity [27]. As a polymer micelle for shell cross-linking, an ABC triblock copolymer with the rational sequence of poly(ethylene glycol)-*b*-poly(L-lysine)-*b*-poly(L-phenylalanine) (PEG-PLys-PPhe) was utilized. In contrast to most CLM systems that are based on non-degradable polyacrylate and polystyrenes, our system is based on PEG and poly(amino acid)s that can be eliminated from the body through renal excretion as non-toxic PEG and degraded amino acid molecules (L-lysine and L-phenylalanine) after drug delivery. PEG-PLys-PPhe is expected to form micelles featuring the PEG corona, the PLys middle shell, and the PPhe inner core. The three domains of the core, the shell, and the corona, are each expected to play a role in generating a useful nanocarrier. The PEG corona enables the prolonged circulation of micelles for effective EPR effects. The PPhe core serves as a reservoir of lipophilic drugs. The PLys middle shells with primary amine groups are used as a specific domain for disulfide cross-linking. The cross-links in the middle shells may not only enhance micellar stability in the blood but also may reduce drug release before the micelles reach the target tissues. Upon endocytosis, the cleavage of disulfide cross-links can be promoted by intracellular GSH to trigger intracellular drug release. Fig. 1 illustrates the key idea and working principle of our disulfide cross-linked micelles as an intracellular carrier of DTX.

The kinetic stability of DTX-loaded disulfide cross-linked micelles (DTX-SSCLM) under serum and micelle-disrupting conditions was investigated to verify the effect of cross-linking for enhancing the stability. The in vivo tissue distribution, tumor targeting ability, and time-dependent excretion profile were also assessed by using a non-invasive, live animal imaging system. In addition, we evaluated the anti-cancer efficacy of DTX-SSCLM in a human breast cancer xenograft model compared with free DTX and DTX-loaded non-cross-linked micelles (DTX-NCLM).

2. Materials and methods

2.1. Materials

α-Methoxy-ω-amino-poly(ethylene glycol) (CH_3O-PEG_{113}-NH_2) with number average molecular weight (M_n) of 5000 g/mol and polydispersity index (PDI) of 1.05 (GPC) was purchased from SunBio Inc. (Seoul, Korea) and used as received. N^6-Carbobenzyloxy-L-lysine (H-Lys(Z)-OH), L-phenylalanine (Phe), triethylamine (TEA), trifluoroacetic acid (TFA), sodium dodecyl sulfate (SDS) and docetaxel (DTX) were purchased from Sigma Co. (St. Louis, MO) and used without further purification. 3,3′-Dithiobis(sulfosuccinimidylpropionate) (DTSSP) was purchased from Pierce (Perbio Science Deutschland GmbH, Bonn, Germany). Monofunctional Cy5.5 *N*-hydroxysuccinimide (NHS) ester was obtained from Amersham Biosciences (Buckinghamshire, UK). *N*,*N*-Dimethylformamide (DMF) and dimethyl sulfoxide (DMSO) were dried and vacuum distilled over calcium hydride. N^6-Carbobenzyloxy-L-lysine *N*-carboxyanhydride (Lys(Z)-NCA) and L-phenylalanine *N*-carboxyanhydride (Phe-NCA) of high purity were synthesized by the Fuchs–Farthing method using triphosgene [28]. Anal. Calcd for Lys(Z)-NCA ($C_{15}H_{18}N_2O_5$): C, 58.82; H, 5.92; N, 9.15. Found: C, 58.72; H, 5.97; N, 9.08. Calcd for Pha-NCA ($C_{10}H_9NO_3$): C, 62.82; H, 4.74; N, 7.33. Found: C, 62.42; H, 4.81; N, 7.28.

2.2. Synthesis of PEG_{113}-$PLys_{19}$-$PPhe_{24}$ triblock copolymer (PEG_{113}-$PLys_{19}$-$PPhe_{24}$)

PEG_{113}-$PLys_{19}$-$PPhe_{24}$ that has EG units of 113, Lys units of 19, and Phe units of 24 was synthesized by a procedure established in our laboratory [27]. In brief, to a stirred solution of CH_3O-PEG_{113}-NH_2 (3 g, 0.6 mmol) in dry DMF (30 mL) was added Lys(Z)-NCA (4.595 g, 15 mmol) at 35 °C under nitrogen. After 24 h, Phe-NCA (2.868 g, 15 mmol) and dry DMF (60 mL) were added to the reaction mixture, and the reaction was maintained for further 24 h. PEG_{113}-$PLys(Z)_{19}$-$PPhe_{24}$ was isolated by repeated precipitation from DMF into diethyl ether. Yield: 86%. In order to remove Z groups. PEG_{113}-$PLys(Z)_{19}$-$PPhe_{24}$ (1 g) was treated with TFA (10 mL) and HBr/HOAc (0.5 mL). PEG_{113}-$PLys_{19}$-$PPhe_{24}$ was isolated by dialysis using a membrane (molecular weight cut-off (MWCO): 1000) for 24 h, followed by freeze-drying.

2.3. Preparation of DTX-loaded micelles with disulfide shell cross-links (DTX-SSCLM)

DTX-loaded PEG_{113}-$PLys_{19}$-$PPhe_{24}$ micelles with shell-specific disulfide cross-links were prepared by the dialysis method and a subsequent shell cross-linking reaction. PEG_{113}-$PLys_{19}$-$PPhe_{24}$ (20 mg) was dissolved in 0.5 mL of DMF at 70 °C, and DTX (2 mg) was subsequently added. The solution was stirred for 6 h at room temperature and then dialyzed against doubly distilled water using a membrane (Spectrapor, MWCO: 1000). After 24 h, the solution of DTX-loaded micelles was collected. DTSSP as a disulfide-containing cross-linking agent was then added to this solution at the feed molar ratio of [DTSSP]:[Lys] = 1:1. The reaction was maintained for 7 h at pH 9.0, and the solution was dialyzed for 3 h to remove residual DTSSP, unloaded DTX, and reaction by-products. The dialyzate was lyophilized to obtain DTX-SSCLM. For preparation of DTX-NCLM, an identical procedure was employed, except for the DTSSP addition. Consumption of primary amines of Lys units during the cross-linking reaction was quantified using a fluorescamine assay.

The loading contents in micelles and loading efficiency of DTX were measured by HPLC after solubilization of DTX-loaded micelles in DMF. The concentration of DTX was determined by high-performance liquid chromatography (HPLC). The HPLC system consisted of a reverse-phase silica column (SepaxHP-C18, 4.6 × 250 mm, 5 μm, Sepax, USA), a mobile phase of acetonitrile, and 0.05% trifluoroacetic acid in water (60:40 v/v) pumped (LC-20AT, Shimadzu) at a flow rate of 1.0 mL/min at 25 °C. A 20 μL aliquot of sample was injected, and the column effluent was detected at 230 nm with a UV detector (CBM-20A, Shimadzu). The DTX concentrations in the samples were determined using a calibration curve of various DTX concentrations (0.1–100 μg/mL).

2.4. Characterization of the DTX-SSCLM

The zeta potential (ζ) was measured in a phosphate buffered saline (PBS) solution (10 mM, pH 7.4) using a 90 PLUS (Brookhaven Instruments Cooperation, New York, USA) particle size analyzer. Dynamic light scattering measurements were performed using a 90 Plus particle size analyzer (Brookhaven Instruments Corporation). The scattered light of a vertically polarized He–Ne laser (632.8 nm) was measured at an angle of 90° and was collected on an autocorrelator. The hydrodynamic diameters (d) of micelles were calculated by using the Stokes–Einstein equation [29]. The polydispersity factor of micelles, represented as μ_2/I^2, where μ_2 is

the second cumulant of the decay function, and Γ is the average characteristic line width, was calculated from the cumulant method [29]. Transmission electron microscopy (TEM) was performed on a JEM-2000EX (JEOL Tokyo, Japan), operating at an acceleration voltage of 200 kV. A drop of sample solution (concentration = 1 g/L) was placed onto a 200-mesh copper grid coated with carbon. About 5 min after deposition, the grid was tapped with a filter paper to remove surface water, followed by air-drying. Negative staining was performed using a droplet of a 5 wt% uranyl acetate solution.

2.5. Stability of the DTX-SSCLM

Kinetic stability of the DTX-SSCLM was investigated in serum-containing or SDS-containing solutions. The effect of SDS or serums on the DTX-SSCLM in aqueous media was estimated by dynamic light scattering analysis. For the stability in serum conditions, the stability of the DTX-SSCLM (3 g/L) in the serum-containing PBS solution (50% fetal bovine serum (FBS)) was examined by dynamic light scattering. At predetermined time periods, the mean diameter of the micelles was monitored, and scattered light intensity (SLI) was compared to the initial scattered light intensity (SLI_0) by dynamic light scattering analysis. For SDS treatment, a SDS solution (1 mL, 7.5 g/L) was added to the DTX-SSCLM solution (2 mL, 0.75 g/L), and the solution was stirred at 500 rpm. At predetermined time periods, the ratio of scattered light intensity (SLI/SLI_0) was monitored. For comparison, the stability of DTX-NCLM was estimated under the same conditions.

2.6. Glutathione-mediated controlled release of DTX

In order to examine the cross-linking effect, the DTX release profiles from the DTX-SSCLM and the DTX-NCLM were compared in the PBS solution. For the effect of GSH on the release of DTX, the DTX-SSCLM in the PBS solution (1 mL, 1 g/L, pH 7.4) was placed in a dialysis membrane bag (MWCO = 1000). The release experiment was initiated by placing the dialysis bag in release media of various GSH concentrations (without GSH, 0.2 μM, and 10 mM). The release medium was shaken at a speed of 100 rpm at 37 °C. At predetermined time intervals, samples (10 mL) were withdrawn and replaced with an equal volume of the fresh medium. The concentration of DTX in the samples was measured by HPLC at 230 nm. The assay for DTX was based on a linear standard curve obtained using the concentration range of 0.1–100 μg/mL.

2.7. Cytotoxicity of the DTX-SSCLM

MDA-MB231 human breast cancer cells were originally obtained from the American Type Culture Collection (Rockville, MD) and cultured in RPMI 1640 (Gibco, Grand Island, NY) containing 10% (v/v) FBS (Gibco) and 1% (w/v) penicillin–streptomycin in a humidified atmosphere of 5% CO_2 at 37 °C.

In vitro cytotoxicity of free DTX, DTX-NCLM, and DTX-SSCLM was evaluated by measuring the half maximal inhibitory concentration (IC_{50}) using the CCK assay [17]. MDA-MB231 cells were seeded at a density of 5×10^3 cells/well in 96-well flat-bottomed plates, and allowed to adhere for 24 h. The medium of each well was then replaced by 200 μL of fresh medium containing free DTX, the DTX-NCLM, and the DTX-SSCLM at various DTX concentrations from 0.01 to 100 μg/mL, and then the plates were incubated (37 °C, 5% CO_2). After 24 h, the medium was removed, and cells were washed with the fresh medium, followed by the CCK assay. The IC_{50} value was calculated as the concentration of DOX yielding 50% inhibition of cell proliferation, compared to the untreated control.

2.8. Preparation of Cy5.5-labeled micelle-forming PEG_{113}-$PLys_{19}$-$PPhe_{24}$

For real-time monitoring of in vivo tissue distribution, time-dependent excretion profile, and tumor accumulation of the DTX-SSCLM, Cy5.5 was labeled to the PLys middle block of micelle-forming PEG_{113}-$PLys_{19}$-$PPhe_{24}$. For conjugation of Cy5.5

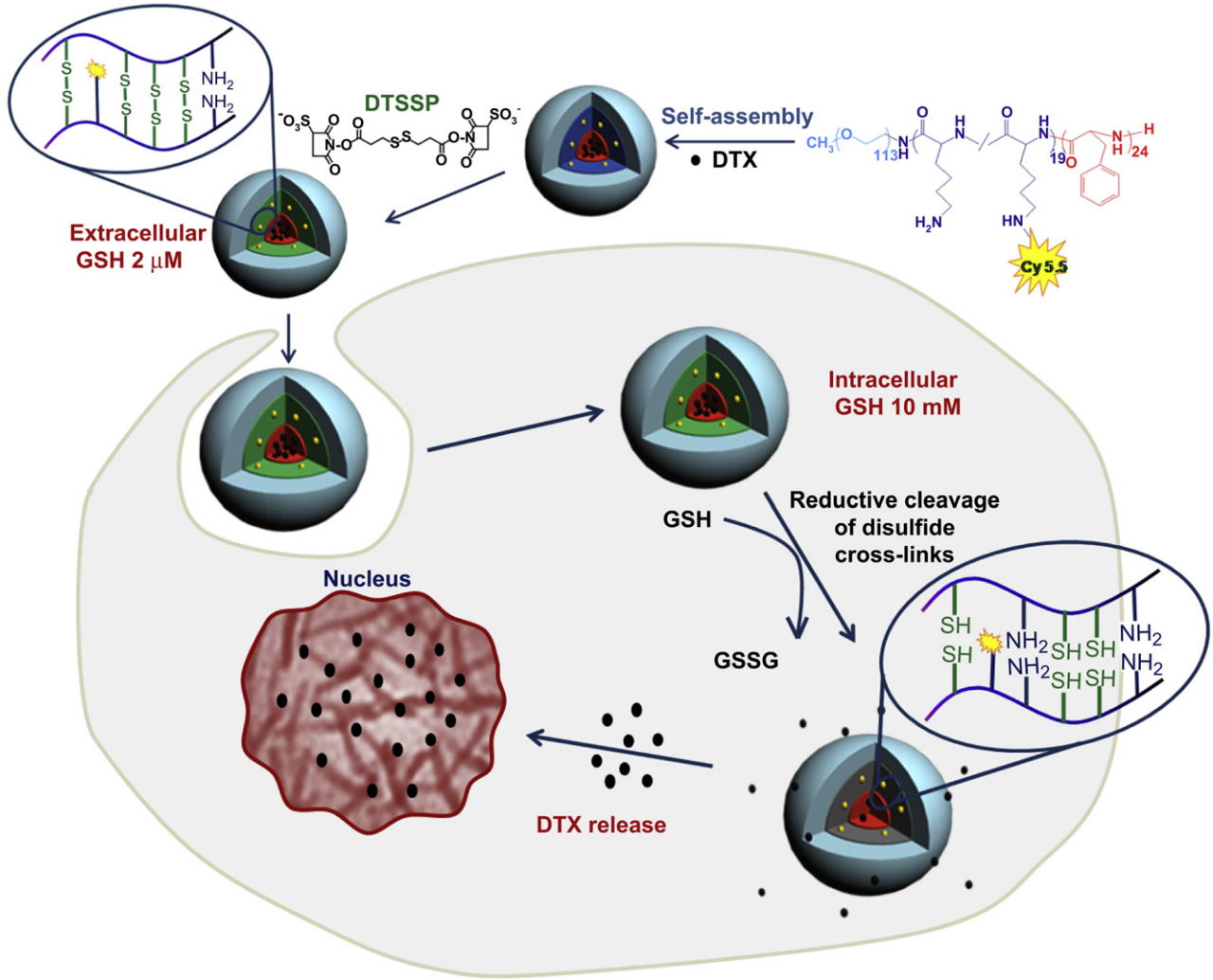

Fig. 1. Illustration of shell cross-linking of DTX-loaded polymer micelles with a redox-labile disulfide cross-links and triggered release of DTX by intracellular GSH.

to the middle PLys block, the molar ratio of Cy5.5 NHS ester to PEG_{113}-$PLys_{19}$-$PPhe_{24}$ was 1:10. Cy5.5 NHS ester (10.3 mg, 0.009 mmol) was added to a stirred solution of PEG_{113}-$PLys_{19}$-$PPhe_{24}$ (1 g, 0.09 mol) and TEA (18 mg, 0.18 mmol) in dry DMF (10 mL) at room temperature in the dark. After 15 h, unbound Cy5.5 NHS ester and by-products were removed by dialysis using a membrane (MWCO: 3500) for 30 h. Finally, Cy5.5-PEG_{113}-$PLys_{19}$-$PPhe_{24}$ was isolated by lyophilization.

2.9. Non-invasive monitoring of in vivo biodistribution and tumor accumulation of the DTX-SSCLM

For non-invasive in vivo optical imaging experiment, the MDA-MB231 human breast cancer were grown in 7-week-old male athymic nude mice (20 g, Institute of Medical Science, Tokyo) by inoculating 1.0×10^7 MDA-MB231 cells into the dorsal side of mice. When tumors grew to approximately 200 ± 30 mm^3 in volume, the tumor accumulation ability of DTX-SSCLM (5 mg/kg in 100 μL of saline) was investigated. To monitor in vivo characteristics of the Cy5.5-labelded DTX-SSCLM (Cy5.5-DTX-SSCLM), 4 wt% of DTX was encapsulated into Cy5.5-labeled PEG_{113}-$PLys_{19}$-PPhe24, followed by the cross-linking reaction with disulfide-containing DTSSP. The shell cross-linking procedure described in the Section 2.3 of Materials and methods was identically utilized. In order to evaluate the effect of shell domain-specific cross-linking on the tumor accumulation. The Cy5.5-labeled DTX-loaded NCLM without shell cross-links (DTX = 4 wt%) was prepared for comparison. After i.v. injection of the Cy5.5-DTX-SSCLM (5 mg/kg in 100 μL of saline), the time-dependant in vivo biodistribution and tumor accumulation ability of the Cy5.5-DTX-SSCLM in an MDA-MB231 human breast tumor-bearing mice were non-invasively imaged using the eXplore Optix System (Advanced Research Technologies Inc., Montreal, Canada). The mouse was automatically moved into the imaging chamber for scanning. Laser power and count time settings were optimized at 25 μW and 0.3 s per point. Excitation and emission spots were raster-scanned in 1 mm steps over the selected region of interest to generate emission wavelength scans. A 670 nm pulsed laser diode was used to excite the Cy5.5 molecules. The NIRF at 700 nm was collected and detected through a fast photomultiplier tube (Hammamatsu, Japan) and a time-correlated single photon counting system (Becker and Hickl GmbH, Berlin, Germany). The in vivo characteristics of the Cy5.5-DTX-SSCLM were confirmed by measuring the NIRF intensity in MDA-MB231 tumor-bearing mice ($n = 3$). Data were calculated by using the region of interest (ROI) function of the Analysis Workstation software (Advanced Research Technologies). To compare tissue and tumor distributions of the Cy5.5-DTX-SSCLM, mice were sacrificed after the 2 days post-injection of the Cy5.5-DTX-SSCLM. The major organs including liver, lung, spleen, kidney, and heart, as well as the tumor, were dissected from the mice, and their fluorescence intensities were determined by using a 12-bit CCD camera (Image Station 4000 MM; Kodak, New Haven, CT) equipped with a special C-mount lens and a Cy5.5 bandpass emission filter (680–720 nm; Omega Optical). Identical illumination settings (e.g., lamp voltage, filter, exposure time) were used in all animal imaging experiments. A quantification of in vivo tumor specificity of the DTX-SSCLM was measured as total photon counts per centimeter squared per steradian (p/s/cm^2/sr) per each tumor ($n = 3$ mice per group).

2.10. Antitumor efficacy of the DTX-SSCLM in tumor-bearing mice

All animal treatments and surgical procedures followed approved protocols and were performed in accordance with the Institutional Animal Care and Use Committee at Kyung Hee University. The antitumor efficacy of the DTX-SSCLM was evaluated in tumor-bearing mice, which were prepared by inoculating a suspension of 1.0×10^7 MDA-MB231 human breast cancer cells in physiological saline (100 μL) into the subcutaneous dorsa of athymic C3H/HeN male mice (7 weeks old, 20–25 g, five mice per group, Institute of Medical Science, Tokyo). When tumors grew to approximately 50–100 mm^3, the mice of six groups were treated with one of the following treatments: (i) normal saline (the control group, $n = 5$); (ii) NCLM (the control group, $n = 5$); (iii) SSCLM (the control group, $n = 5$); (iv) free DTX at 3 mg/kg ($n = 5$); (v) DTX-NCLM at 3 mg DTX/kg ($n = 5$); (vi) DTX-SSCLM at 3 mg DTX/kg ($n = 5$). Each sample was injected once every 3 day for 15 days. Tumor volumes were calculated as $a \times b^2/2$, where a and b are the largest and smallest diameter, respectively.

2.11. Immunohistological analysis

Apoptotic and non-apoptotic cells in tumor tissues were histologically evaluated using the 4′,6-diamidino-2-phenylindole (DAPI) and terminal transferase dUTP nick-end labeling (TUNEL) assays, with a commercial apoptosis detection kit (MILLIPORE, MA, USA) with the following modifications. Samples were fixed with 4% para-formaldehyde (methanol-free) for 10 min at room temperature. The samples were washed with PBS twice for 5 min each time and then incubated with 0.2% Triton X-100 for 15 min at room temperature. After the samples were washed twice more with PBS for 5 min each time, they were incubated with equilibration buffer from the MILLIPORE Kit for 10 min at room temperature. The equilibration buffer was drained and a reaction buffer containing equilibration buffer, nucleotide mix, and TdT enzyme was added to the tissue sections, which then were incubated in a dark, humidified atmosphere at 37 °C for 1 h. The reaction was terminated by immersing the samples in 2× standard saline citrate for 15 min, and the samples then were washed three times for 5 min each to remove unincorporated rhodamine-TdT. The apoptotic cells in tissues were determined by TUNEL assay and the slides were counterstained with DAPI. TUNEL data were analyzed by a researcher blind to the nature, at ×400 magnification, using a computer-aided light microscope.

2.12. Statistical analysis

The statistical significance of differences between experimental and control groups was determined using a student's t-test. P values <0.05 were considered significant, and significant differences are shown by asterisks in the Figures.

3. Results and discussion

3.1. Preparation and characterization of DTX-loaded PEG-PLys-PPhe core-shell-corona micelles

As a self-assembling block copolymer for the core-shell-corona polymer micelles, the PEG_{113}-$PLys_{19}$-$PPhe_{24}$ copolymer was synthesized via the one-pot two-step polymerization of Lys(Z)-NCA and Phe-NCA in the presence of a CH_3O-PEG-NH_2 macroinitiator and a subsequent deprotection process. The molar composition ratio of the monomeric repeating units in PEG, PLys, and PPhe was 45:19:24. The conversion of monomeric Lys(Z) and Phe to polymeric PLys(Z) and PPhe was found to be 76% and 96%, respectively (Table 1). The M_n of PEG_{45}-$PLys_{19}$-$PPhe_{24}$, calculated by ^{1}H NMR, was 11,000 g/mol. Gel permeation chromatography (GPC) analyses showed a narrow molecular weight distribution ($M_w/M_n = 1.08$). It is known that N-carboxyanhydride (NCA)-based polymerization for poly(amino acid) follows a pseudo-living polymerization when the ratio of the monomer to the amine-based initiator ($[M]_0/[I]_0$) is around 20 [30]. The choice of starting PEG ($M_w/M_n = 1.05$) with a narrow molecular weight distribution and the inherent feature of NCA polymerization may afford such a narrow molecular weight distribution of PEG_{45}-$PAsp_8$-$PPhe_{19}$. PEG_{45}-$PLys_{19}$-$PPhe_{24}$ self-assembled to form core-shell-corona polymer micelles with three well-defined, distinct domains: the inner hydrophobic PPhe core, the anionic PAsp middle shell, and the solvated PEG outer corona. Docetaxel (DTX) was loaded into PEG_{45}-$PAsp_8$-$PPhe_{19}$ micelles by a dialysis method. The loading content and the loading efficiency were 4.0 wt% and 40%, respectively. The mean hydrodynamic diameter was 62.8 nm. The zeta potential (ζ) of the DTX-loaded PEG_{45}-$PAsp_8$-$PPhe_{19}$ micelles was reasonably positive ($\zeta = 19.3$ mV).

3.2. Formation of DTX-loaded disulfide cross-linked micelles (DTX-SSCLM)

DTX-loaded disulfide cross-linked micelles were prepared by adding DTSSP to an aqueous solution of DTX-loaded PEG_{113}-$PLys_{19}$-$PPhe_{24}$ micelles. Water-soluble DTSSP cross-linkers with activated

Table 1
Characteristics of the PEG_{113}-$PLys_{19}$-$PPhe_{24}$ copolymer.

Copolymer	Feed ratio ([EG]:[Lys(Z)]:[Phe])	Composition ratio[a] ([EG]:[Lys]:[Phe])	Conversion of Lys(Z)[a] (%)	Conversion of Phe[a] (%)	M_n[a]	M_w/M_n[b]
PEG_{113}-$PLys_{19}$-$PPhe_{24}$	113:25:25	113:19:24	76	96	11,000	1.08

[a] Calculated by ^{1}H NMR spectra.
[b] Estimated by GPC.

Table 2
The micelle sizes, zeta potentials, and polydispersity factors of various micelles.

Micelles	d^a (nm)	Zeta potential[b] (mV)	μ_2/I^{2c}
DTX-NCLM	62.8	19.3	0.29
DTX-SSCLM	58.8	2.1	0.28

[a] Mean hydrodynamic diameters at 25 °C.
[b] Estimated at pH 7.4 at 25 °C.
[c] Polydispersity factor estimated by dynamic light scattering.

bifunctional *N*-hydroxysuccinimide esters reacted with the primary amines of PLys middle shells to form intramicellar cross-links. After the cross-linking reaction, 75.6% of the primary amines of the PLys shells were converted to amide linkages, as calculated by a fluorescamine assay. Notably, after the shell cross-linking, the value of the positive zeta potential of DTX-NCLM was decreased from 19.3 mV to 2.1 mV (Table 2). This decreased zeta potential reflects the conversion of primary amine groups of the middle PLys shells to amide linkages formed during the shell cross-linking reaction. The DTX-SSCLM maintained a reasonable size of precursor polymer micelles (DTX-NCLM) with a moderate distribution. Interestingly, the shell cross-linking decreased the mean diameter of the micelles, which reflects the condensed structure as a result of chemical network formation in the micellar middle shells (Table 2). TEM images show the spherical nature of DTX-loaded polymer micelles and that the shell cross-linking reaction did not induce intermicellar aggregation. The TEM results are consistent with the results observed by dynamic light scattering (Fig. 2); this indicates that the PEG outer corona confines the shell cross-linking reaction within the PAsp middle shells and prevents the formation of intermicellar aggregates.

3.3. Effects of shell cross-linking on the stability of the DTX-SSCLM

The stability of drug-loaded micelles in the blood has been an issue of great significance because it is one of the major factors for the successful delivery to target tissues [26,31]. When administered systemically by intravenous injection, a drug carrier encounters plasma proteins and blood cells before it reaches target tissues. It was reported that many components in the blood, particularly the serum proteins, interacted with drug carriers and tended to alter the stability and the tissue disposition of the carriers. Thus, if the nanocarrier cannot maintain its integrity in the presence of blood components, efficient drug delivery to the target tissues cannot be accomplished.

We estimated the stability of DTX-SSCLM in serum conditions. It is well known that the monitoring of the scattered light intensity of micelles is an appropriate technique to estimate the micelle stability in solutions. The stability of DTX-SSCLM in the serum solution (50% fetal bovine serum (FBS)) was estimated based on a literature method [31]. As shown in Fig. 3a, the DTX-SSCLM maintained long-term stability in the serum-containing solution, which was determined by observing the scattering light intensity and constant mean diameter. The loss of scattered light intensity of the DTX-SSCLM was not to a great extent, and 85% of the initial intensity was maintained after 2 h.

However, the DTX-NCLM without shell cross-links exhibited a dramatic loss of scattered light intensity. Within 30 min, the scattered light intensity decreased to 49% of the initial intensity. This finding indicates the dissociation of a large portion of polymer micelles in the serum solution. This tendency is consistent with the previous report, in which FBS significantly destabilized the

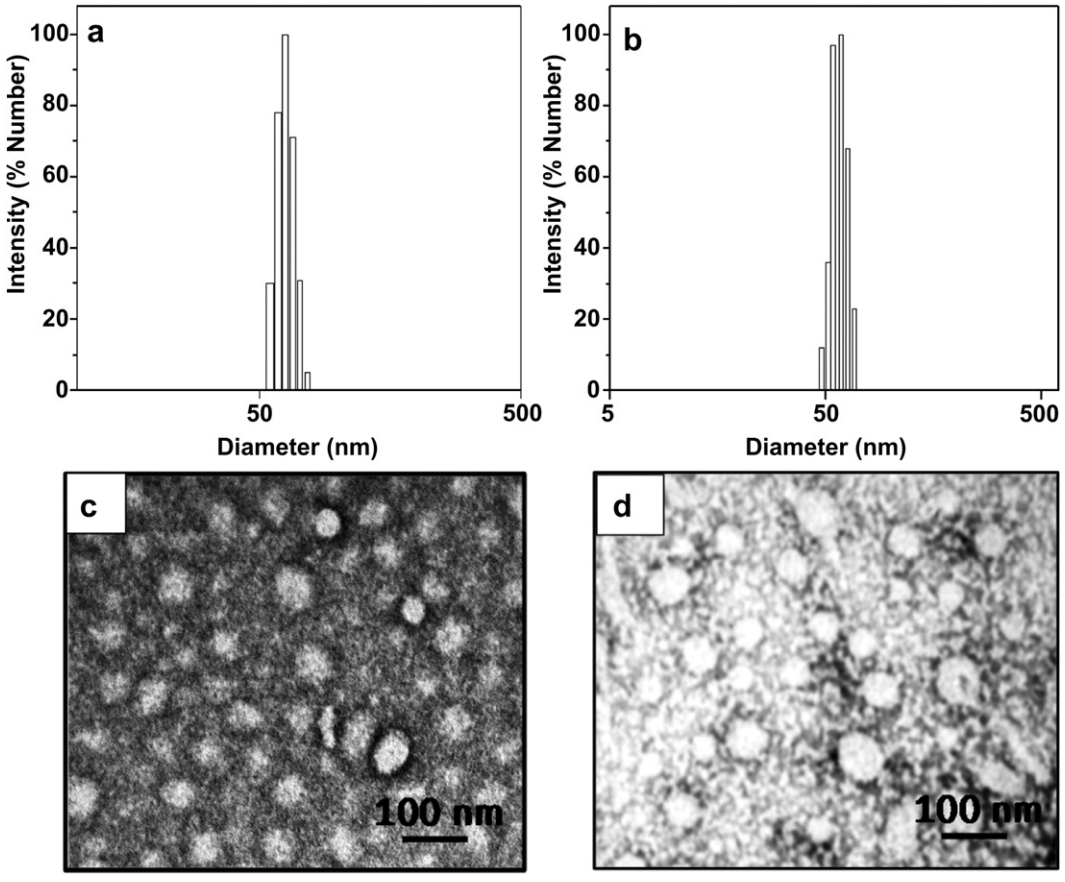

Fig. 2. Size distributions and morphology of DTX-NCLM (a and c) and DTX-SSCLM (b and d) estimated by dynamic light scattering and TEM. Scale bars = 100 nm.

camptothecin-loaded PEG-b-poly(benzyl aspartate) copolymer micelles [31]. The constant diameter that was detected for the DTX-NCLM was probably due to the remaining polymer micelles at the observation time period.

Monitoring the micellar stability in the presence of SDS has been established as a general method to evaluate the micellar stability [7,26,32]. Thus, we also estimated the stability of DTX-SSCLM in the presence of sodium dodecyl sulfate (SDS), a strong micelle-disrupting agent. The kinetic stability of the DTX-SSCLM and the DTX-NCLM was monitored in the presence of SDS. For the DTX-NCLM, the relative scattering intensity was dramatically decreased to 50% after 2 h, which indicates the SDS-induced dissociation of the micelle structure (Fig. 3b). In contrast, the DTX-SSCLM maintained more than 90% of the initial scattering intensity after 3 h. This tendency of the DTX-SSCLM was consistent with the results that were observed with the serum solutions. This finding indicates that the DTX-SSCLM can remain their assembled integrity even in the harsh conditions for micelle dissociation because the shell cross-linkers cause the polymer micelles to be resistant to the SDS effects. Although the analytical tools to assess the in vivo stability of the DTX-SSCLM were not developed, we confirmed the enhanced stability in the serum and SDS solutions. Due to their thermodynamically frozen assembled structure, the

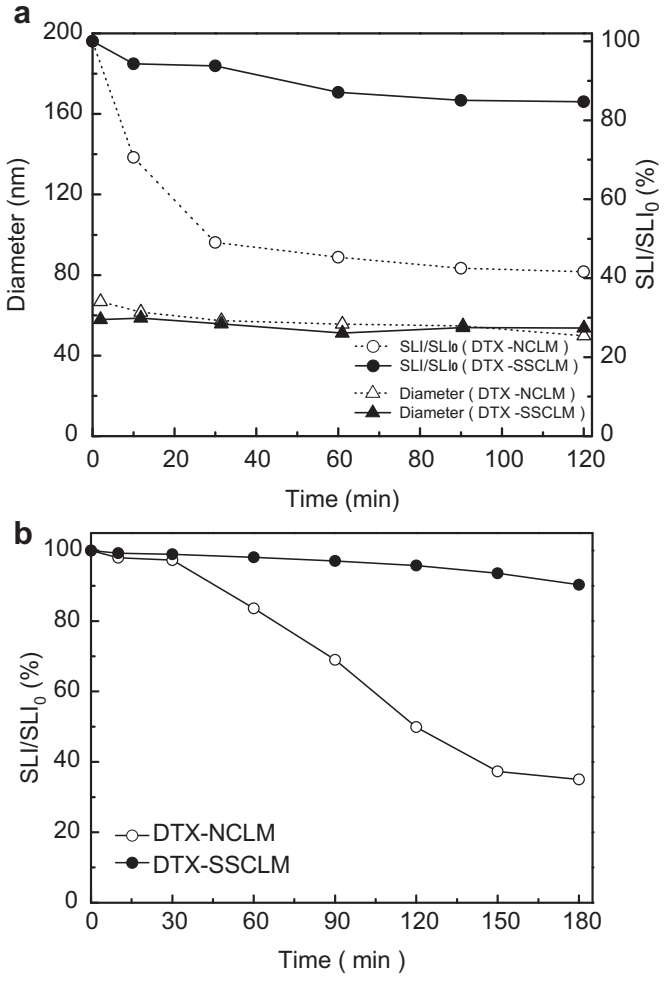

Fig. 3. (a) Time-dependent changes of the mean diameter and the ratio of scattered light intensities (SLI/SLI_0 (%)) of DTX-SSCLM and DTX-NCLM in the FBS-containing PBS solution (50% FBS). (b) Kinetic changes in relative scattered light intensity (SLI/SLI_0) for DTX-SSCLM and DTX-NCLM in the presence of SDS (2.5 g/L).

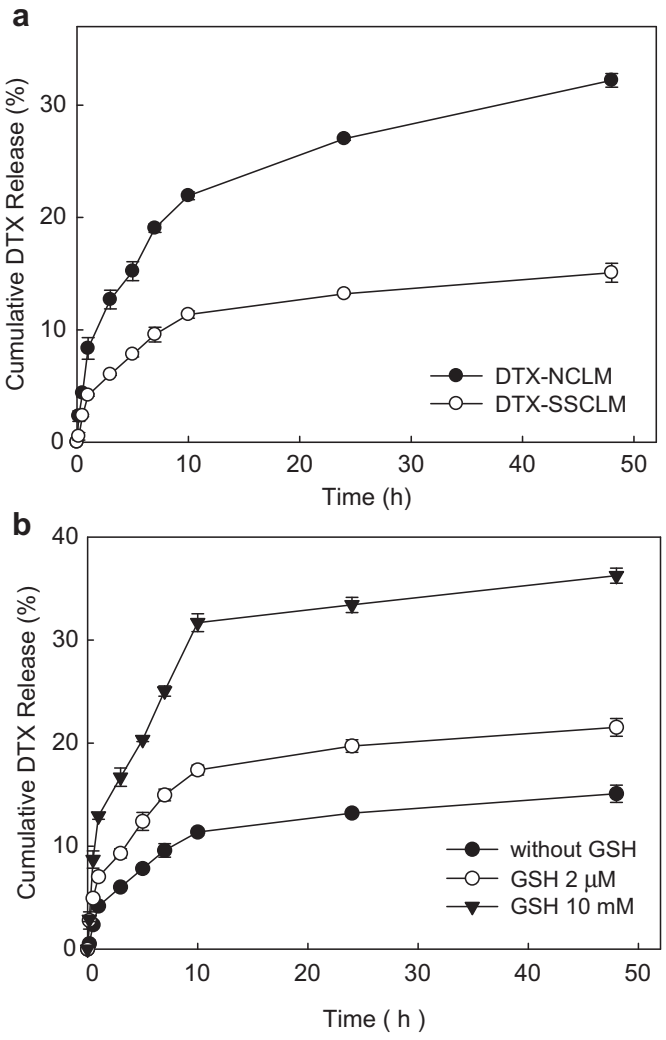

Fig. 4. (a) DTX release from DTX-NCLM and DTX-SSCLM at the PBS solution (pH 7.4). (b) GSH-controlled DTX release from DTX-SSCLM as a function of the GSH concentration. Each point represents the mean value of n experiments ± S.D. ($n = 3$).

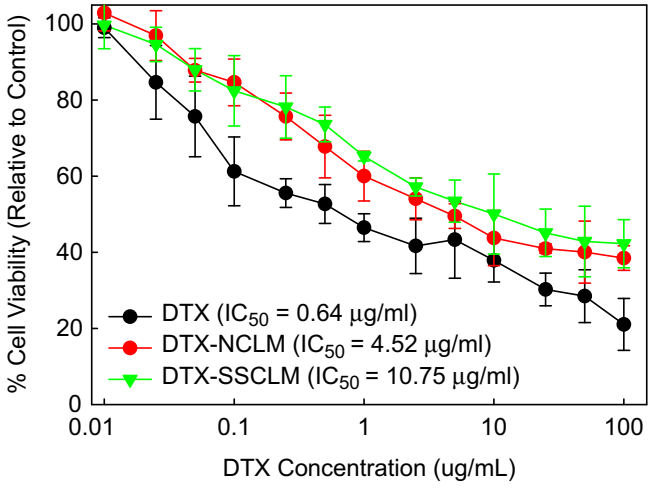

Fig. 5. In vitro cytotoxicity of DTX, DTX-NCLM, DTX-SSCLM for MDA-MB231 cells after 24 h ($n = 3$).

DTX-SSCLM may serve as a robust carrier, as compared with the non-cross-linked DTX-NCLM.

3.4. Redox-responsive controlled drug release from the DTX-SSCLM

To estimate the effect of the disulfide cross-links on the DTX release, we examined the DTX release from the DTX-SSCLM and the DTX-NCLM in the PBS solution. As shown in Fig. 4a, the released amount of entrapped DTX in the PBS solution was greatly reduced for the DTX-SSCLM, in comparison with the DTX-NCLM. Although the shell cross-linking did not totally block the release of DTX from DTX-SSCLM, it effectively inhibited the DTX release. The shell cross-links of the DTX-SSCLM can act as a diffusion barrier for the DTX release, thereby resulting in a lower release rate and amount. At 24 h, 27.0% of the loaded DTX was released from the DTX-NCLM, whereas 13.2% of DTX was released from the DTX-SSCLM; this indicated that the shell cross-links led to a 48.9% reduction of the DTX release. This result may support our assumption that the diffusion-limited cross-linked layer would minimize the loss of the entrapped drug in the blood. Next, we were interested in knowing whether the DTX release is facilitated in response to an intracellular reducing GSH level. Fig. 4b exhibits the DTX release profiles from DTX-SSCLM at different GSH concentrations. At the extracellular GSH level (2 μM), the DTX release rate from DTX-SSCLM was rather increased. This indicates that the low GSH level in the blood may induce damage of the disulfide cross-links to a certain degree, but not to a great extent. Noticeably, as the GSH concentration increased to the cytoplasm level (10 mM), the DTX release was

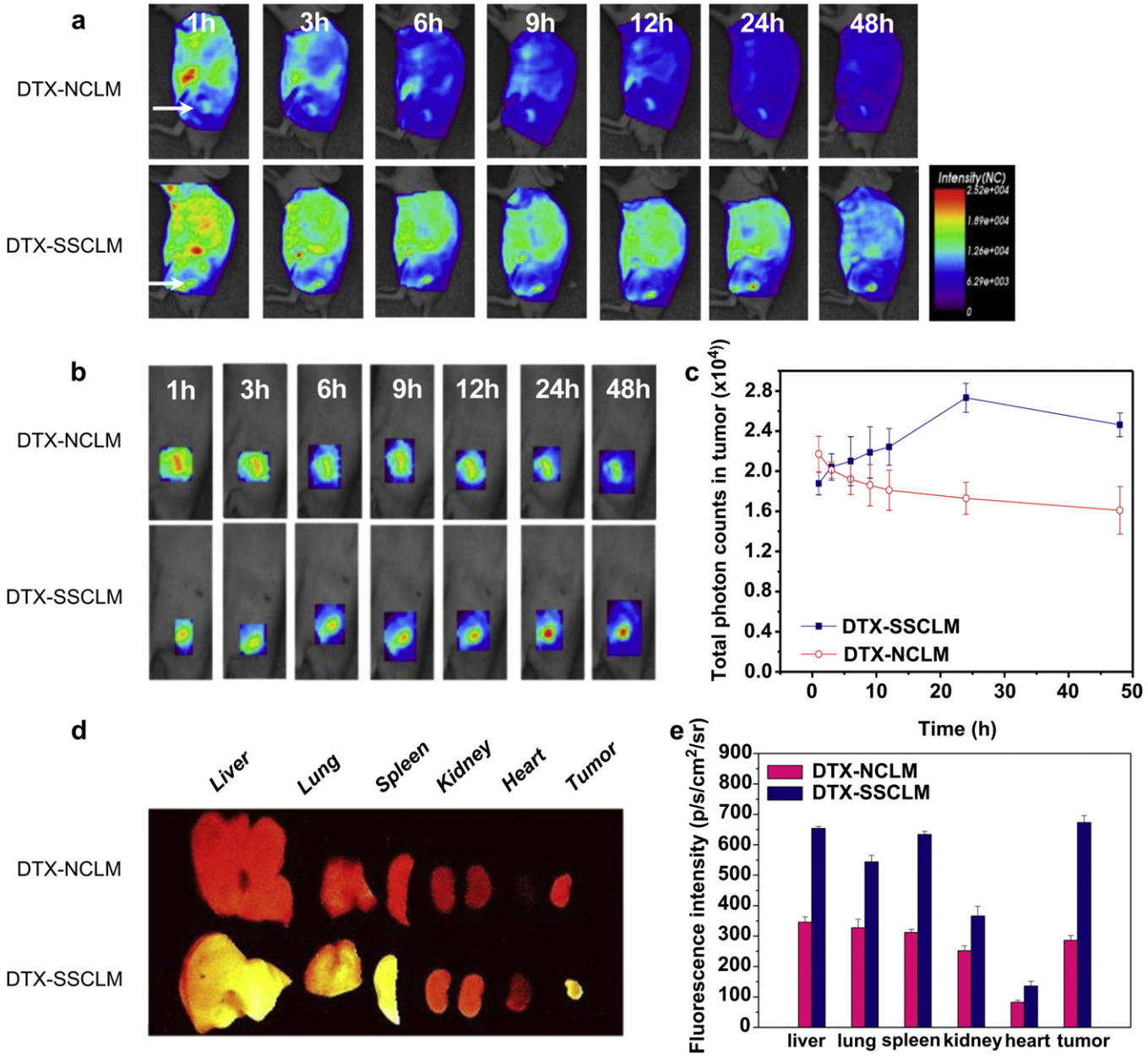

Fig. 6. (a) In vivo non-invasive NIRF images of time-dependent whole body imaging of MDA-MB231 tumor-bearing mice after i.v. injection of Cy5.5-DTX-NCLM and Cy5.5-DTX-SSCLM. Solid arrows indicate the tumors. (b) In vivo tumor specificity of DTX-NCLM and DTX-SSCLM (c) The total NIRF photon counts per centimeter squared per steradian (p/s/cm^2/sr) per each tumor ($n = 3$ mice per group) as a function of time. (d) Ex vivo NIRF imaging of isolated normal organs (liver, lung, spleen, kidney and heart) and tumors excised at 3 days post-injection of Cy5.5-DTX-NCLM and Cy5.5-DTX-SSCLM. (e) A quantification of in vivo biodistribution of DTX-NCLM and DTX-SSCLM was recorded as total photon counts per centimeter squared per steradian (p/s/cm^2/sr) per each excised organ at 3 days post-injection in MDA-MB231 tumor-bearing mice ($n = 3$ mice per group). All data represent means ± S.D. ($n = 3$).

facilitated much more than it was at the blood level GSH concentration. At 24 h, the DTX release from the DTX-SSCLM at 10 mM GSH was increased by 69.5%, compared with the release at the 2 μM GSH level. This result indicates that, at a cellular GSH level, the cleavage of the disulfide linkages is more pronounced to accelerate the release of DTX. These DTX-SSCLM not only minimize the drug loss at the extracellular environments, but also they release drugs for therapeutic effects once they are located within the target cells. In terms of the therapeutic efficiency, the use of DTX-SSCLM would be more promising than the use of DTX-NCLM without disulfide cross-links.

3.5. In vitro cytotoxicity of the DTX-SSCLM

The in vitro cytotoxicities of the DTX-SSCLM and the DTX-NCLM in MDA-MB231 human breast cells were estimated. As shown in Fig. 5, the DTX-SSCLM exhibited relatively low toxicity ($IC_{50} = 10.75$ μg/mL) in comparison with free DTX ($IC_{50} = 0.64$ μg/mL) and DTX-NCLM ($IC_{50} = 4.52$ μg/mL). At an identical incubation period, the disulfide cross-linked DTX-SSCLM had slightly lower toxicity than the DTX-NCLM. In the case of non-cross-linked DTX-NCLM, drug release was initiated immediately upon placement of the DTX-NCLM in the cell culture media. The DTX release rate from the DTX-SSCLM was slower than that of the DTX-NCLM, because the DTX release from the DTX-SSCLM was accelerated after the breakage of disulfide cross-links by GSH within the cytosol. Therefore, the lower toxicity of the DTX-SSCLM could be explained. Using in vitro experiments, we confirmed that the DTX-SSCLM maintains the cytotoxicity of native DTX-NCLM by releasing DTX within the cells. The potential for minimizing drug loss to the blood and for enhanced accumulation in the tumor tissue, due to the robust nature of the DTX-SSCLM, may enhance its overall therapeutic efficacy in vivo, relative to free DTX and non-cross-linked DTX-NCLM.

3.6. Preparation of the Cy5.5-labeled DTX-SSCLM for in vivo non-invasive imaging

One of the specific aims of this work is to determine whether the shell-specific cross-linking of core-shell-corona micelles can improve the carrier properties of native core-shell-corona micelles with a simple assembled structure, in terms of the prolonged circulation and the enhanced tumor accumulation. To assess the in vivo distribution, Cy5.5, a NIRF dye was labeled within PLys shell domains of the DTX-SSCLM. The conjugation ratio of Cy5.5 to the polymer chain was 0.7:1, as determined by using the extinction coefficient of Cy5.5 at 675 nm (2.5×10^5 M^{-1} cm^{-1}) [33]. This low ratio is systematically considered for the maintenance of large portions of primary amines for disulfide cross-linking with PLys in the shell domains. Considering the ratio of Cy5.5 molecules (0.7 per one polymer chain), the ratio of residual primary amines for disulfide cross-linking was 18.3 per the polymer chain (96.3% of the initial primary amines), which is enough for the shell cross-linking reaction. After the cross-linking reaction, 80.2% of the primary amines within the PLys shell domains were converted to amide linkages, as calculated by a fluorescamine assay. This result indicates that a large portion of the Lys units participates in the shell cross-linking. For micelle assembly, the ratio of Cy5.5-conjugated polymers to non-conjugated polymers was 1:50. It is known that the NIRF of Cy5.5 was self-quenched when the Cy5.5 molecules contacted each other within the localized environments [34]. Therefore, the control of the polymer ratio is to minimize the number of localized Cy5.5 molecules within the cross-linked PLys shells and to monitor the tissue distribution by minimizing the reduction of the NIRF of the Cy5.5 molecules.

3.7. In vivo biodistribution and tumor accumulation of the DTX-SSCLM

For real-time monitoring of the in vivo biodistribution of the DTX-SSCLM, Cy5.5-labeled DTX-SSCLM was intravenously injected into MDA-MB231 human breast tumor-bearing mice, and a time-dependent biodistribution was observed by using non-invasive NIRF imaging in live animals. Within 1 h after the i.v. administration, strong NIRF signals were observed in the whole body within 1 h post-injection, which indicates the rapid circulation of DTX-NCLM and DTX-SSCLM in the blood stream (Fig. 6a). For the non-cross-linked DTX-NCLM, the NIRF gradually decreased and became negligible after 12 h. On the other hand, the DTX-SSCLM exhibited a strong fluorescence signal in the body for up to 2 days, which was possibly due to the prolonged circulation characteristics of the DTX-SSCLM with stabilized cross-linked structures

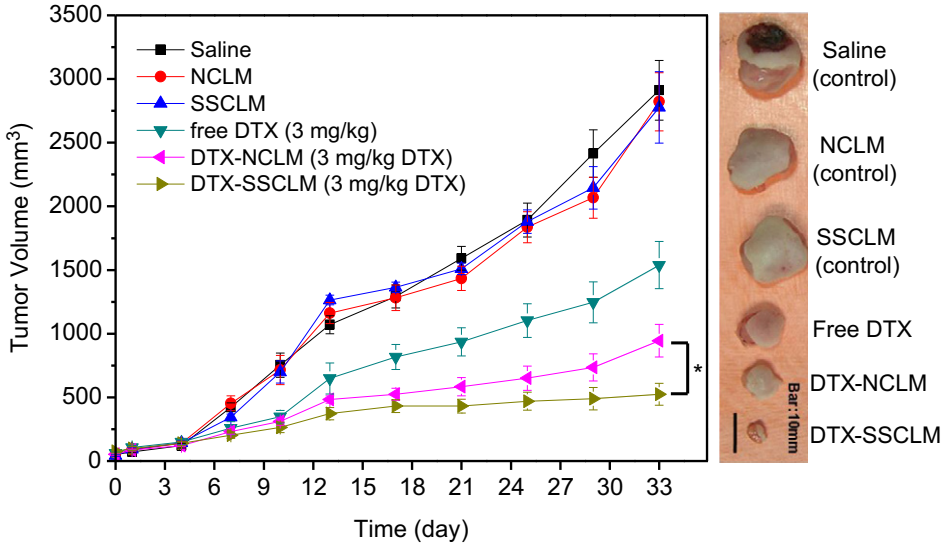

Fig. 7. Changes in tumor volumes after injection of saline, NCLM, SSCLM, free DTX, DTX-NCLM (4.0 wt% DTX), and DTX-SSCLM (4.0 wt% DTX), respectively. The results represent the means ± S.D. ($n = 6$). *$P < 0.05$.

compared with the DTX-NCLM. Within 3 h post-injection, the DTX-SSCLM was primarily localized in the liver tissue, and some of the DTX-SSCLM were accumulated in the tumor tissue. After 6 h, the fluorescence signal in the liver gradually decreased. Fig. 6b shows the tumor specificity of the DTX-SSCLM compared with that of the DTX-NCLM. It is noteworthy that the NIRF signal in the tumor tissue gradually increased up to 1 day and maintained its strong signal up to 2 days, which resulted from the enhanced tumor accumulation of the DTX-SSCLM. This enhanced tumor accumulation can be explained by the excellent serum stability of the DTX-SSCLM. The total photon counts of the DTX-SSCLM in the tumor tissue gradually increased for 1 day and maintained a strong signal even at 2 days. The photon counts from the tumors of DTX-NCLM-treated mice decreased upon i.v. administration and exhibited weak signals throughout the observation periods. At 48 h, the photon count of the DTX-SSCLM in the tumor tissue was 57% higher than that of the DTX-NCLM-treated mice (Fig. 6c). This low tumor accumulation of non-cross-linked DTX-NCLM may be due to their low stability in the blood stream and the gradual dissociation of the majority of the DTX-NCLM. For this reason, we could not expect the EPR effect from the DTX-NCLM for effective tumor targeting. To provide substantial evidence of the tumor specificity of the DTX-SSCLM, the major organs (liver, lung, spleen, kidney, heart, and tumor tissues) were isolated at 3 days post-injection and ex vivo images of each organ were observed (Fig. 6d). The strongest NIRF intensity was found on the tumor tissues; this indicated that the DTX-SSCLM was predominantly accumulated in the tumor tissue, although a large portion of the DTX-SSCLM was also localized in the liver and spleen (Fig. 6e). For the DTX-NCLM, a similar distribution pattern was found, but the total NIRF signals in the organs were much lower than those from the DTX-SSCLM, due to the relatively low stability in blood.

3.8. *In vivo antitumor efficacy of the DTX-SSCLM in tumor-bearing mice*

We designed the DTX-SSCLM with an assumption that the disulfide shell cross-links can reduce the DTX leakage and can be disrupted to facilitate the DTX release within target tumor cells, thereby improving the anti-cancer therapeutic efficacy. To evaluate the antitumor efficacy of the DTX-SSCLM, DTX-SSCLM and DTX-free or DTX-containing control groups was injected, every three days,

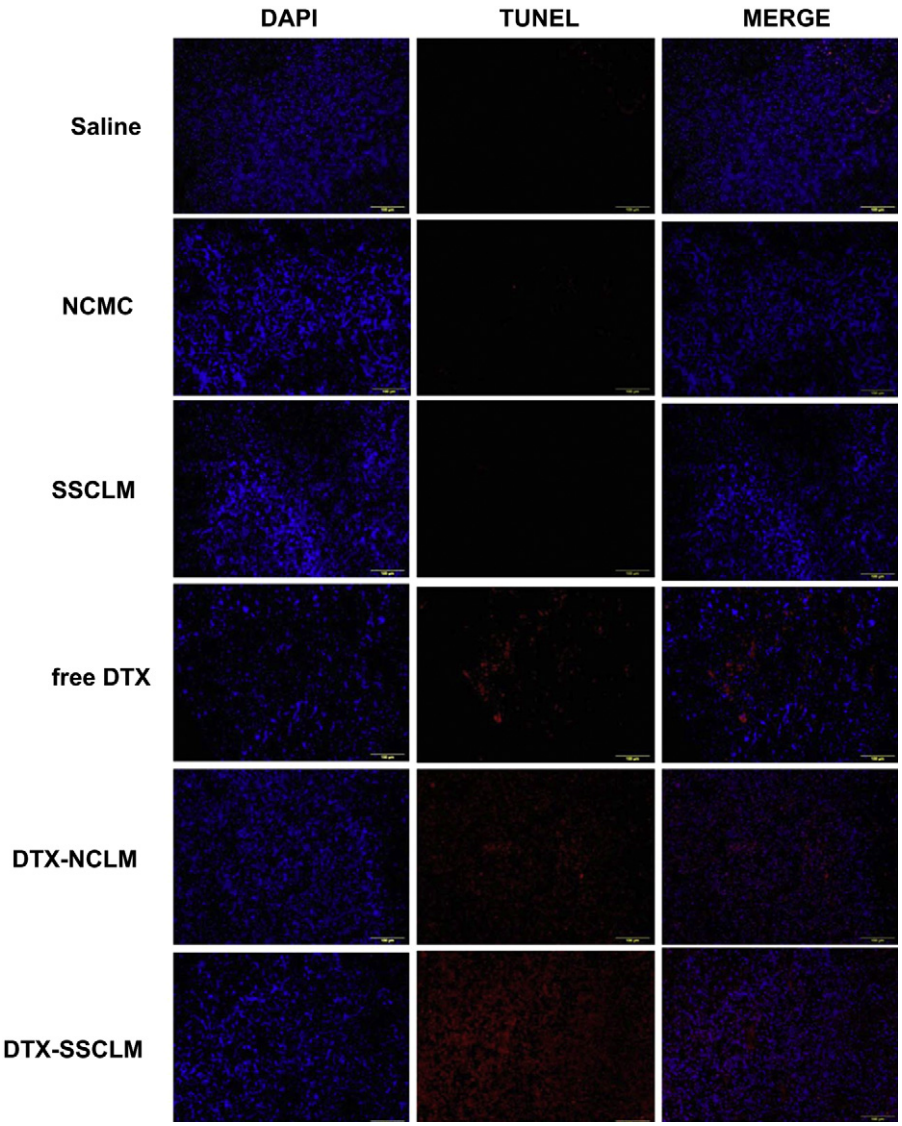

Fig. 8. TUNEL immunostain of apoptotic cells in MDA-MB231 human breast tumor xenografts growing in athymic nude mice treated with saline, NCLM, SSCLM, free DTX, DTX-NCLM (4.0 wt% DTX), and DTX-SSCLM (4.0 wt% DTX), respectively.

into MDA-MB231 human breast tumor-bearing mice via the lateral tail vein.

Fig. 7 shows the changes in tumor volumes in the C3H/HeN male mice after intravenous administration of saline, NCLM, SSCLM, free DTX, DTX-NCLM, and DTX-SSCLM. Neither saline nor DTX-free micelle (NCLM and SSCLM) treatments had any substantial effect on the tumor growth, and the tumor volumes increased rapidly. The treatment with free DTX was effective in tumor regression to some extent, but it did not have efficacy that was comparable to the DTX-NCLM and the DTX-SSCLM. The DTX-SSCLM is significantly more efficacious in tumor reduction, as compared with non-cross-linked DTX-NCLM. As shown in Fig. 7, there were no significant differences in the sizes of the tumors between the DTX-NCLM treatment group and the DTX-SSCLM-treated group until 10 days post-injection. However, after the administration for 12 days, the tumor volume was remarkably more decreased in the DTX-SSCLM-treated group. At 33 days after injection, the average tumor volume in the DTX-SSCLM-treated mice had increased relatively slowly and had reached only 500 mm^3, whereas the average tumor volume in the DTX-NCLM-treated mice had reached 900 mm^3; this indicates that the DTX-SSCLM exhibited enhanced anti-cancer activity over the DTX-NCLM by 44.4% in terms of tumor volume regression. One reason for the enhanced in vivo efficacy might be explained by the enhanced accumulation of the DTX-SSCLM at the tumor site due to the EPR effect that was positively affected by the prolonged circulation. In addition, the effective protection of DTX within the core domains against the rapid clearance before tumor targeting and the subsequent intracellular release of DTX may contribute to the enhanced antitumor efficacy.

3.9. Histological analysis

The antitumor efficacy of DTX-SSCLM against MDA-MB231 tumors growing in C3H/HeN mice was also evaluated by the TUNEL immunohistological assay, which visualizes apoptotic cells in tumor tissues. Fig. 8 shows images of DAPI staining (nuclei), TUNEL staining (apoptosis), and a merge of the two images for tumors treated with saline, NCLM, SSCLM, free DTX, DTX-NCLM, and DTX-SSCLM after 35 days. The apoptotic cell nuclei were barely detectable in the control animals treated with saline and DTX-free micelles (NCLM and SSCNM), but apoptotic nuclei were clearly present in the tumors of mice treated with free DTX, DTX-NCLM, and DTX-SSCLM. Notably, more apoptotic cells were found in the tumor tissues treated with DTX-SSCLM than in the tumor tissues treated with free DTX and DTX-NCLM. This tendency for apoptotic analysis is consistent with the results of in vivo antitumor efficacy (Fig. 7).

4. Conclusions

We have demonstrated that the DTX-loaded core-shell-corona micelles with disulfide shell cross-links (DTX-SSCLM) exhibited enhanced tumor accumulation and antitumor therapeutic efficacy, as compared with the non-cross-linked counterpart (DTX-NCLM). DTX-SSCLM maintained their robust structure in serum and in strong destabilization conditions (SDS). The introduction of redox-labile disulfide cross-links into the middle shell of PEG-PLys-PPhe micelles may meet the major requirements of targeted nano-carriers with high delivery efficiency and low toxicity: i) high stability in the blood stream due to the stable disulfide cross-links, ii) prolonged blood circulation due to the PEG outer corona (minimized uptake by RES), iii) ability to reduce drug loss before reaching target tissues by the cross-linked diffusion barrier, iv) the enhanced EPR effect, v) facilitated drug release within target cells by dissociation of disulfide cross-links, and vi) the excretion from the body as non-toxic PEG and amino acids (L-lysine and L-phenylalanine). The domain-specific cross-linking within the core-shell-corona micelles may provide useful tools for enhancing the antitumor efficacy of existing or newly developed micelles such as polymer micelles and nano-aggregates.

Acknowledgments

This research was supported by Basic Science Research Program through the National Research Foundation of Korea (NRF) funded by the Ministry of Education, Science and Technology (2010-0007721) and the Fundamental R&D Program for Core Technology of Materials (K0006028) by Ministry of Knowledge Economy, Korea.

References

[1] Kim SH, Jeong JH, Lee SH, Kim SW, Park TG. Local and systemic delivery of VEGF siRNA using polyelectrolyte complex micelles for effective treatment of cancer. J Control Release 2008;129:107–16.
[2] Oh KT, Yin H, Lee ES, Bae YH. Polymeric nanovehicles for anticancer drugs with triggering release mechanisms. J Mater Chem 2007;17:3987–4001.
[3] Lee Y, Fukushima S, Bae Y, Hiki S, Ishii T, Kataoka K. A protein nanocarrier from charge-conversion polymer in response to endosomal pH. J Am Chem Soc 2007;129:5362–3.
[4] Convertine AJ, Diab C, Prieve M, Paschal A, Hoffman AS, Johnson PH, et al. pH Responsive polymeric micelle carriers for siRNA drugs. Biomacromolecules 2010;11:2904–11.
[5] Mikhail AS, Allen C. Polyethylene glycol-*b*-polycaprolactone micelles containing chemically conjugated and physically entrapped docetaxel: synthesis, characterization and the influence of the drug on micelle morphology. Biomacromolecules 2010;11:1273–80.
[6] Shiraishi K, Kawano K, Minowa T, Maitani Y, Yokoyama M. Preparation and in vivo imaging of PEG-poly(L-lysine)-based polymeric micelle MRI contrast agents. J Control Release 2009;136:14–20.
[7] Lee HJ, Kim SE, Kwon IK, Park C, Kim C, Yang J, et al. Spatially mineralized self-assembled polymeric nanocarriers with enhanced robustness and controlled drug-releasing property. Chem Commun 2010;46:377–9.
[8] Han SY, Han HS, Lee SC, Kang YM, Kim IS, Park JH. Mineralized hyaluronic acid nanoparticles as a robust drug carrier. J Mater Chem 2011;21:7996–8001.
[9] Choi KY, Min KH, Yoon HY, Kim KM, Park JH, Kwon IC, et al. PEGylation of hyaluronic acid nanoparticles improves tumor target ability in vivo. Biomaterials 2011;32:1880–9.
[10] Du Y, Weng Q, Yuan H, Hu FQ. Synthesis and antitumor activity of stearic acid-g-dextran copolymeric micelles for intracellular doxorubicin delivery. ACS Nano 2010;4:6894–902.
[11] Talelli M, Rijcken CJF, van Nostrum CF, Storm G, Hennink WE. Micelles based on HPMA copolymers. Adv Drug Deliv Rev 2010;62:231–9.
[12] Kawaguchi T, Honda T, Nishihara M, Yamamoto T, Yokoyama MJ. Histological study on side effects and tumor targeting of a block copolymer micelle on rats. J Control Release 2009;136:240–6.
[13] Talelli M, Iman M, Varkouhi AK, Rijcken CJF, Schiffelers RM, Etrych T, et al. Core-crosslinked polymeric micelles with controlled release of covalently entrapped doxorubicin. Biomaterials 2010;31:7797–804.
[14] Lee SC, Kim C, Kwon IC, Chung H, Jeong SY. Polymeric micelles of poly(2-ethyl-2-oxazoline)-block-poly(ε-caprolactone) copolymer as a carrier for paclitaxel. J Control Release 2003;89:437–46.
[15] Lee SW, Chang DH, Shim MS, Kim BO, Kim SO, Seo MH. Ionically fixed polymeric nanoparticles as a novel drug carrier. Pharm Res 2007;24:1508–16.
[16] Ko J, Park K, Kim YS, Kim MS, Han JK, Kim K, et al. Tumoral acidic extracellular pH targeting of pH-responsive MPEG-poly(beta-amino ester) block copolymer micelles for cancer therapy. J Control Release 2007;123:109–15.
[17] Lee SJ, Min KH, Lee HJ, Koo AN, Rim HP, Jeon BJ, et al. Ketal cross-linked poly(ethylene glycol)-poly(amino acid)s copolymer micelles for efficient intracellular delivery of doxorubicin. Biomacromolecules 2011;12:1224–33.
[18] Jones DP, Carlson JL, Samiec PS, Sternberg P, Mody VC, Reed RL, et al. Glutathione measurement in human plasma: evaluation of sample collection, storage and derivatization conditions for analysis of dansyl derivatives by HPLC. Clin Chim Acta 1998;275:175–84.
[19] Takae S, Miyata K, Oba M, Ishii T, Nishiyama N, Itaka K, et al. PEG-detachable polyplex micelles based on disulfide-linked block catiomers as bioresponsive nonviral gene vectors. J Am Chem Soc 2008;130:6001–9.
[20] Song N, Liu W, Tu Q, Liu R, Zhang Y, Wang J. Preparation and in vitro properties of redox-responsive polymeric nanoparticles for paclitaxel delivery. Colloids Surf B Biointerfaces 2011;87:454–63.
[21] Zhao M, Biswas A, Hu B, Joo KI, Wang P, Gu Z, et al. Redox-responsive nanocapsules for intracellular protein delivery. Biomaterials 2011;32:5223–30.
[22] Matsumoto S, Christie RJ, Nishiyama N, Miyata K, Ishii A, Oba M, et al. Environment-responsive block copolymer micelles with a disulfide cross-

linked core for enhanced siRNA delivery. Biomacromolecules 2009;10:119–27.
[23] Zhang L, Liu W, Lin L, Chen D, Stenzel MH. Degradable disulfide core-cross-linked micelles as a drug delivery system prepared from vinyl functionalized nucleosides via the RAFT process. Biomacromolecules 2008;9:3321–31.
[24] Chan Y, Wong T, Byrne F, Kavallaris M, Bulmus V. Acid-labile core cross-linked micelles for pH-triggered release of antitumor drugs. Biomacromolecules 2008;9:1826–36.
[25] Chan Y, Bulmus V, Zareie M, Byrne F, Barner L, Kavallaris M. Acid-cleavable polymeric core-shell particles for delivery of hydrophobic drugs. J Control Release 2006;115:197–207.
[26] Li Y, Xiao K, Luo J, Xiao W, Lee JS, Gonik AM, et al. Well-defined reversible disulfide cross-linked micelles for on-demand paclitaxel delivery. Biomaterials 2011;32:6633–45.
[27] Koo AN, Lee HJ, Kim SE, Chang JH, Park C, Kim C, et al. Disulfide-cross-linked PEG-poly(amino acid)s copolymer micelles for glutathione-mediated intracellular drug delivery. Chem Commun 2008;48:6570–2.
[28] Daly WH, Poché D. The preparation of *N*-carboxyanhydrides of α-amino acids using bis (trichloromethyl)carbonate. Tetrahedron Lett 1988;29:5859–62.
[29] Harada A, Kataoka K. Novel polyion complex micelles entrapping enzyme molecules in the core: preparation of narrowly-distributed micelles from lyzosome and poly(ethylene glycol)-poly(aspartic acid) block copolymers in aqueous medium. Macromolecules 1998;31:288–94.
[30] Deming T. Facile synthesis of block copolypeptides of defined architecture. Nature 1997;390:386–9.
[31] Opanasopit P, Yokoyama M, Watanabe M, Kawano K, Maitani Y, Okano T. Influence of serum and albumins from different species on stability of camptothecin-loaded micelles. J Control Release 2005;104:313–21.
[32] Kang N, Perron MÉ, Prud'homme RE, Zhang Y, Gaucher G, Leroux JC. Stereocomplex block copolymer micelles: core-shell nanostructures with enhanced stability. Nano Lett 2005;5:315–9.
[33] Min KH, Park K, Kim YS, Bae SM, Lee S, Jo HG, et al. Hydrophobically modified glycol chitosan nanoparticles-encapsulated camptothecin enhance the drug stability and tumor targeting in cancer therapy. J Control Release 2008;127:208–18.
[34] Kim K, Lee M, Park H, Kim JH, Kim S, Chung H, et al. Cell-permeable and biocompatible polymeric nanoparticles for apoptosis imaging. J Am Chem Soc 2006;128:3490–1.